The Engineering Society
For Advancing Mobility
Land Sea Air and Space®
400 COMMONWEALTH DRIVE WARRENDALE, PA 15096

SAE Technical Paper Series

880278

Parametric Analysis of Resistance Spot Welding Lobe Curve

E. W. Kim and T. W. Eagar
Massachusetts Institute of Technology

International Congress and Exposition
Detroit, Michigan
February 29-March 4, 1988

880278

Parametric Analysis of Resistance Spot Welding Lobe Curve

E. W. Kim and T. W. Eagar

Massachusetts Institute of Technology

ABSTRACT

A linearized lumped parameter heat balance model was developed and is discussed for the general case of resistance welding to see the effects of each parameter on the lobe shape. The parameters include material properties, geometry of electrodes and work piece, weld time and current, and electrical and thermal contact characteristics. These are then related to heat dissipation in the electrodes and the work piece.

The results indicate that the ratio of thermal conductivity and heat capacity to electrical resistivity is a characteristic number which is representative of the ease of spot weldability of a given material. The increases in thermal conductivity and heat capacity of the sheet metal increase the lobe width while increases in electrical resistivity decrease the lobe width.

Inconsistencies in the weldability of thin sheets and the wider lobe width at long welding times can both be explained by the heat dissipation characteristics. These are mainly a function of the ratio of electrode diameter to the square of the work piece thickness.

RESISTANCE SPOT WELDING involves complicated interactions between the physical and metallurgical properties of the material and electomagnetic and mechanical phenomena of the process. From a manufacturing point of view, it is very important to establish consistent welding procedures for practical welding. Due to the complexity of the interactions among the various parameters, methods of establishing these procedures for new materials and new equipment have usually been empirical. Even for a material with the same designation, weld parameters sometimes have to be reset due to the inconsistencies in the weld behavior [1].

The lobe curve has been used for many years to characterize weldability during resistance spot welding. The weldability of a material in resistance spot welding is determined by two main factors. Firstly, the width of the lobe curve, which shows the permissible weld current range at a constant weld time and secondly the wear of the electrodes. These two factors are controlled by the interplay between the many parameters which govern the temperature distribution in the parts during the welding thermal cycle. Galvanized steel in particular may have narrower lobes and greater electrode wear when compared with uncoated steels.

A number of analytical and numerical models have been developed to understand the mechanism of nugget formation [2-9]. Although the models have attempted to incorporate the complexities of the weld parameters, such as temperature dependent material properties and contact resistances, these models offer very limited explanations about the effect of each parameter on the weld lobe curve. This seems to be partly due to ill-defined phenomena (e.g. as the contact resistance at the interfaces). It may also be due to the orientation of the research which is mostly aimed at automatic control of the process [10-16].

In order to understand the basics of weld lobe shape, a research program is being undertaken in the MIT welding laboratory. The main questions to be addressed are what causes the welding lobe curves to be shaped the way they are and what are the important phenomena which influence the lobe curves. As a part of the above mentioned endeavours, a linearized lumped parameter heat balance model was developed for the general case of resistance spot welding. It is hoped that this model will show the effect of each parameter on the lobe curve shape. The variables include the geometry of electrodes and the work pieces, electrical

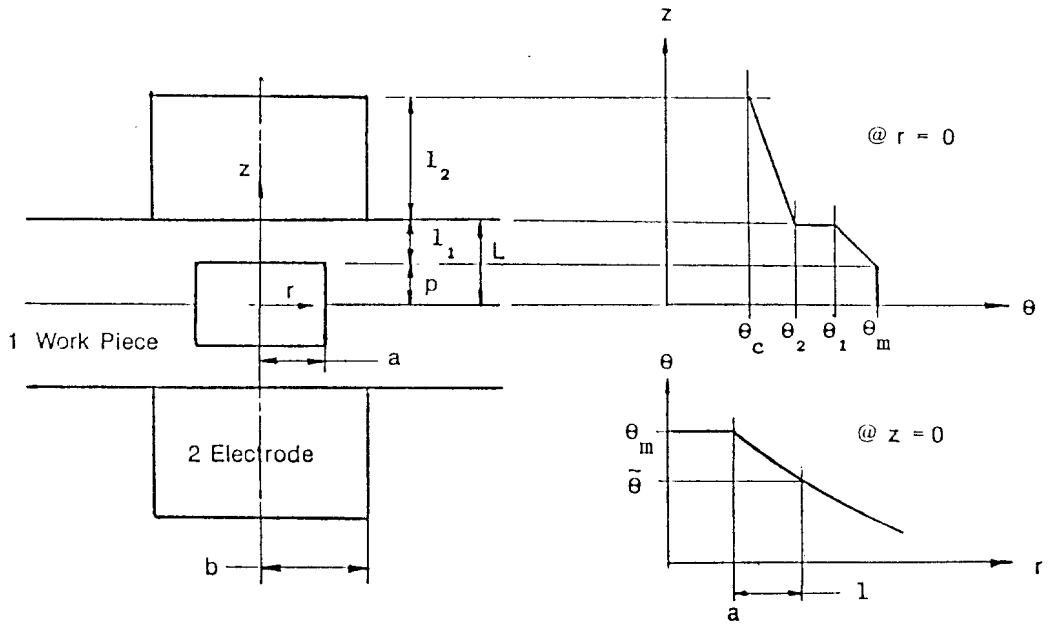

Figure 1: An Approximate Nugget Growth Model with Corresponding Temperature Profiles.

resistance, temperature dependent properties of materials, phase changes and heat dissipation into the cooling water and the surrounding sheet metal. This model was then compared with experimental data to quantify the distribution of heat in the process.

MODEL DEVELPOMENT

The model described in figure 1 was developed to determine the heat balance in the system as a function of nugget growth. A temperature discontinuity at the electrode-work piece interface is assumed. Conduction heat loss through the electrode-work piece interface and into the work piece is estimated as a function of welding time and weld geometry. The overall thermal equilibrium is established by considering a free boundary at the electrode and the work piece surfaces except where they contact. A fixed temperature θ_c, equal to the cooling water temperature is assumed at the internal water cooling surface of the electrode. The size of the work pieces is assumed to be infinite in the radial direction. The nugget shape is assumed to be a disk growing radially and axially in the same proportions as found in a post mortem examination of the maximum nugget size. This assumption is supported by the compuer simulation results found in reference 9. The maximum nugget size is assumed to have 80% penetration and to be equal to the electrode contact diameter. The expulsion limit is assumed to have been reached when the nugget diameter matches the electrode face diameter. The equations are established with lumped parameters.

The total heat generation rate, $\dot{Q}_g$, can be described as

$$\dot{Q}_g = I^2 R \qquad (1)$$

where, $R = R_w + R_c + R_e$

R_w : work piece bulk resistance
R^w : total contact resistance
R^c : electrode resistance
Δt : welding time
I : welding current

The heat of fusion required for nugget formation, h_f, is

$$H_f = H\,\Delta V_n \qquad (2)$$

where, H : heat of fusion per unit volume
ΔV_n : nugget volume ($=\pi a^2 p$)

If the temperature rise in the model is described in the three different regions with lumped quantities, the total heat required is,

$$Q_T = \rho_n C_{pn} \Delta\theta_n \Delta V_n + \rho_s C_{ps} \Delta\theta_s \Delta V_s + \rho_e C_{pe} \Delta\theta_e \Delta V_e = Q_T^n + Q_T^s + Q_T^e \qquad (3)$$

where, ρ : density
C_p : specific heat
V^p : volume
$\Delta\theta$: temperature rise
n : in a nugget
s : in surroundings
e : in electrodes

Thus the total heat balance including the total heat loss rate, $\dot{Q}_L$, through the model boundaries (into the cooling water) can be written as follows.

$$\dot{Q}_g \Delta t = H_f + Q_T + \dot{Q}_L \Delta t \qquad (4)$$

EFFECT OF MATERIAL PROPERTIES

Equation (4) can be rearranged as

$$(I^2 - \dot{Q}_L/R)\Delta t = (H_f + Q_T^n + Q_T^s + Q_T^e)/R \qquad (5)$$

Neglecting both the heat loss and temperature rise in the electrodes and the temperature rise in the surroundings,

$$\epsilon \cdot I^2 R \Delta t = (H + \rho_n C_{pn} \Delta\theta_n)\ \Delta V_n \qquad (6)$$

ϵ : efficiency of heat input

This is basically a lobe curve, which is a hyperbola with axes of welding time, Δt, and the square of the welding current, I. This basic lobe curve may be translated or rotated or distorted by changes in each parameter. The change in one parameter may have effects not only on one term but also on other terms simultaneously. Here the effects are considered in each term separately. The final results will be a combination of these effects.

The nugget volume, ΔV_n, is constant for a certain size of nugget. In this case, equation (6) approaches a constant value. Figure 2 represents equation (6) with two different nugget sizes. The larger nugget size shifts the lobe curve in the direction of higher currents or longer weld times.

The effect of $\rho_n C_{pn}$ and H can be considered in a similar way. Equation (6) also shows the effect of these parameters. Higher values of $\rho_n C_{pn}$ and H shift the lobe curve in a like manner as does a larger size nugget. The temperature dependence of $\rho_n C_{pn}$ will affect the lobe shape as shown in figure 3.

The effect of electric resistance can be considered as follows,

$$I^2 \Delta t = \text{constant}/R \qquad (7)$$

Generally, the dynamic resistance changes in the manner shown in figure 4, at least for steel. Even though R_c drops very fast during the early weld cycles, its contribution to the thermal field seems to be great due to its large magnitude. Higher R_c values will shift the lobe curve farther to the left as shown in figure 5-a. As R_w changes with time (temperature), the slope dR_w/dt will be important in nugget formation as shown in figure 5-b and 5-c. The ratio of R_c to R_w may also affect the nugget growth mechanism due to differences in the heat generation pattern. It is also possible to see the effect of electrode pressure in equation (7). Since higher electrode pressure results in a lower R_c, the lobe curve will shift as in figure 5-a.

The heat required to raise the temperature of the material surrounding the nugget, Q_T^s, and the heat requires to raise the temperature of the electrodes, Q_T^e, can be seen in equation (5). If these terms are added to the right hand side of equation (6), the lobe curve will be shifted in the direction of higher energy input. In equation (5) one can see that the extent of this shift is determined by the ratio of the amount of heat required for heating of the electrode and the work piece divided by the electrical resistance (i.e. the ratio of heat capacity to electrical resistivity, σ). This is an important parameter in the characterization of nugget growth mechanisms and lobe curve.

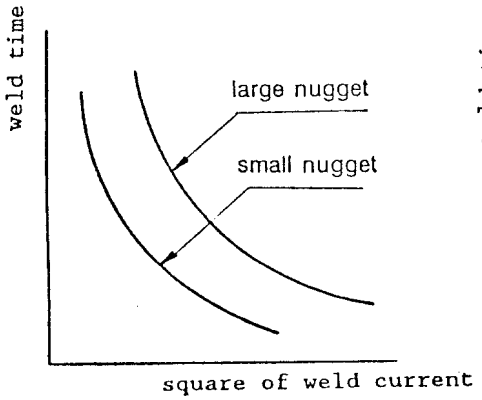

Figure 2: Basic Lobe Curve

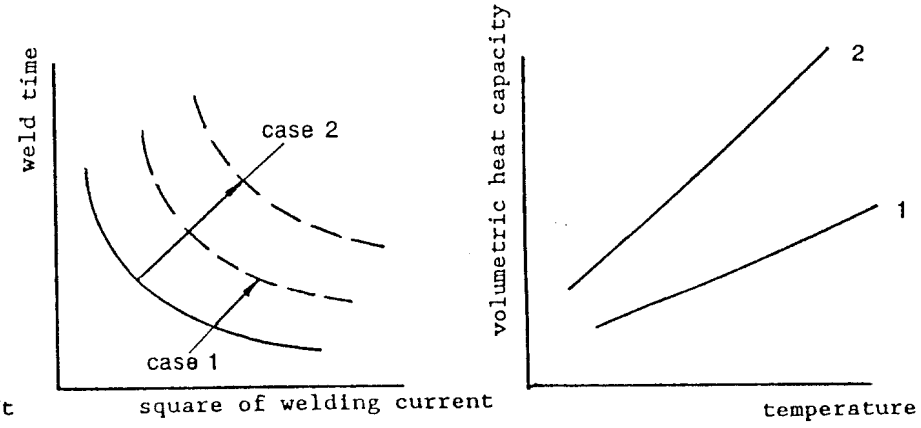

Figure 3: Effect of ρC_p Change.

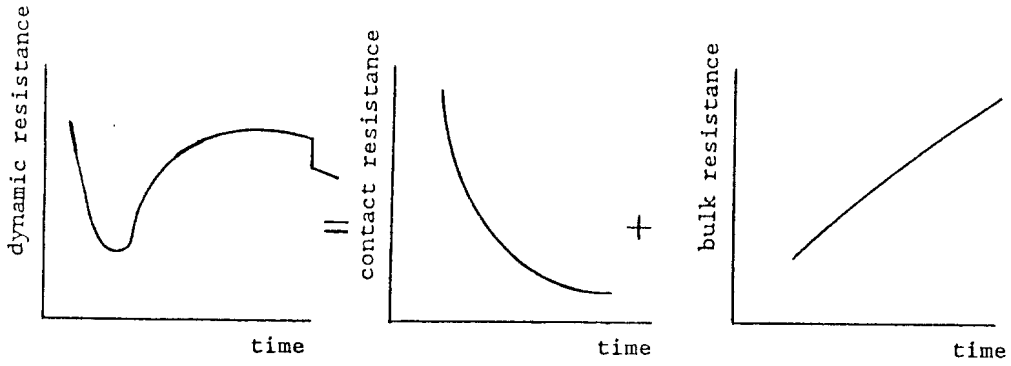

Figure 4: Typical Dynamic Resistance Change

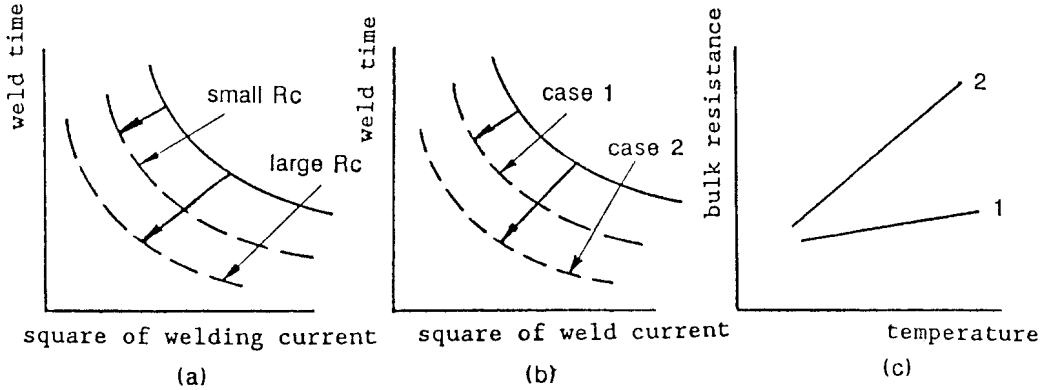

Figure 5: Effect of Resistance Change.

EFFECT OF GEOMETRY AND HEAT LOSS

Considering the total heat loss rate, equation (6) changes to

$$(I^2R-\dot{Q}_L)\Delta t = \text{constant} \qquad (8)$$

This shifts the lobe curve in the high current direction by $\dot{Q}_L/R$, which is actually a function of the thermal properties of the material and of the geometry. This is shown in figure 6. Here, one can see that the ratio of the heat loss rate to the resistance (i.e. the ratio of thermal conductivity to electrical resistivity σ) can be a important parameter in the characterization of nugget growth and weld lobe shape.

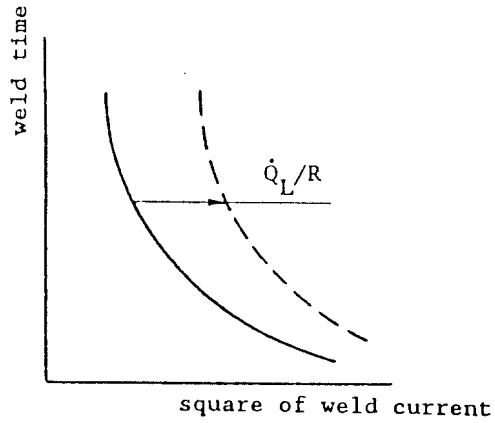

Figure 6: Effect of Heat Loss

The total heat loss rate of the nugget, $\dot{Q}_L^n$, is the sum of the axial heat loss rate through the electrodes, $\dot{Q}_a$, and the radial heat loss rate through the work pieces, $\dot{Q}_r$. The thermal conductivity of the copper electrode is much greater than that of the work piece materials (this is not the case for aluminum welding) and the time scale of the process is on the order of 1/10 second (5 to 20 AC cycles). In this time scale the heat diffusion distance in the electrode is about 3 mm while it is 1 mm in the steel. When the electrode face thickness is very thin (e.g. less than 3 mm) the heat generated in the electrodes and that transferred from the work piece will be carried away by cooling water while the nugget developes. In this case the heat dissipation in the axial direction is influenced by the heat transfer characteristics of the cooling water. If the electrode face thickness is greater than 3 mm, the heat transferred from the work pieces and that generated in electrode itself will be used to heat up the electrodes. Hence a smaller portion of the heat may be car-

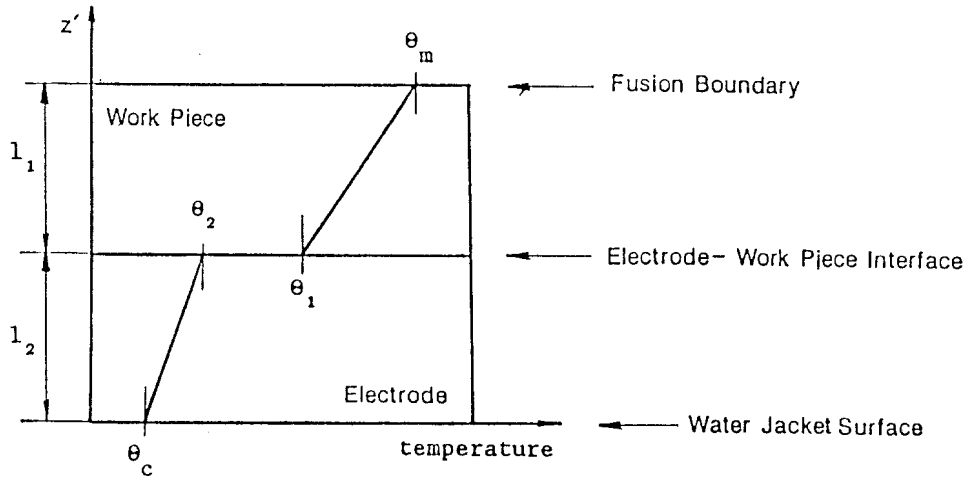

Figure 7: Steady State Temperature Distribution Near a Contact Interface.

ried away by the cooling water during nugget development. In any case, if it is assumed that the temperature build up in the electrodes has already been reached when melting starts in the nugget, the heat flux in the axial direction can be thought to be balanced during nugget growth with θ_1 as a interface temperature at the work piece side. Therefore, the heat loss rate, $\dot{Q}_l$, into the cooling water will be roughly equal to the axial heat loss rate, $\dot{Q}_a$.

The heat loss in the axial direction is assumed to be proportional to the square of the nugget radius. The temperature profile between the interface and the melting front is assumed to be linear. Then the axial loss rate is,

$$\dot{Q}_a = k_1(\theta_m-\theta_1)\pi a^2/l_1 \qquad (9)$$

Where, k_1 : thermal conductivity
θ_m : melting temperature
θ_1 : interface temperature at work piece
l_1 : distance from melting interface to electrode contact surface
a : nugget radius

The heat required for the temperature rise in surrounding nugget material, Q_T^S, is thought to be determined by the heat flux out of the nugget, $\dot{Q}_r$, and the heat generation in surrounding material itself. The temperature distribution in this region is assumed to be mainly determined by $\dot{Q}_r$ when the nugget has grown to sufficient size. If the heat loss through the work piece is assumed to be proportional to the area of the nugget side wall, then,

$$\dot{Q}_r = k_1(\theta_m-\tilde{\theta})2\pi ap/l \qquad (10)$$

Where, $\tilde{\theta}$: characteristic surrounding temperature
l : characteristic heat diffusion length

The thermal conductivity, k_1, included in the heat loss equations changes with temperature while the interface temperature, θ_1, is also affected by geometry and interfacial characteristics. This is also affected by the heat generation pattern due to the electrical resistivity change with temperature.

To see the effect of geometry, a one dimensional model was made in the axial direction as shown in figure 7. A steady state heat flux balance near the electrode-work piece interface is modeled without heat generation included.

For steady state heat flux equilibrium,

$$k_1(\theta_m-\theta_1)/l_1 = k_2(\theta_2-\theta_c)/l_2 = h(\theta_1-\theta_2) \qquad (11)$$

$$\theta_1 = \frac{(k_1k_2+A)\theta_m + (B-k_1k_2)\theta_c}{A+B} \qquad (12)$$

$$\theta_2 = \frac{A\theta_m + B\theta_c}{A+B} \qquad (13)$$

$$\Delta\theta = \frac{k_1k_2(\theta_m-\theta_c)}{A+B} \qquad (14)$$

Where, $A = k_1hl_2$, $B = k_1k_2 + k_2hl_1$

Plots of these equations are shown in figure 8. This model shows that the interface temperature changes with nugget growth, which is represented by l_1. Figure 8-b is exactly

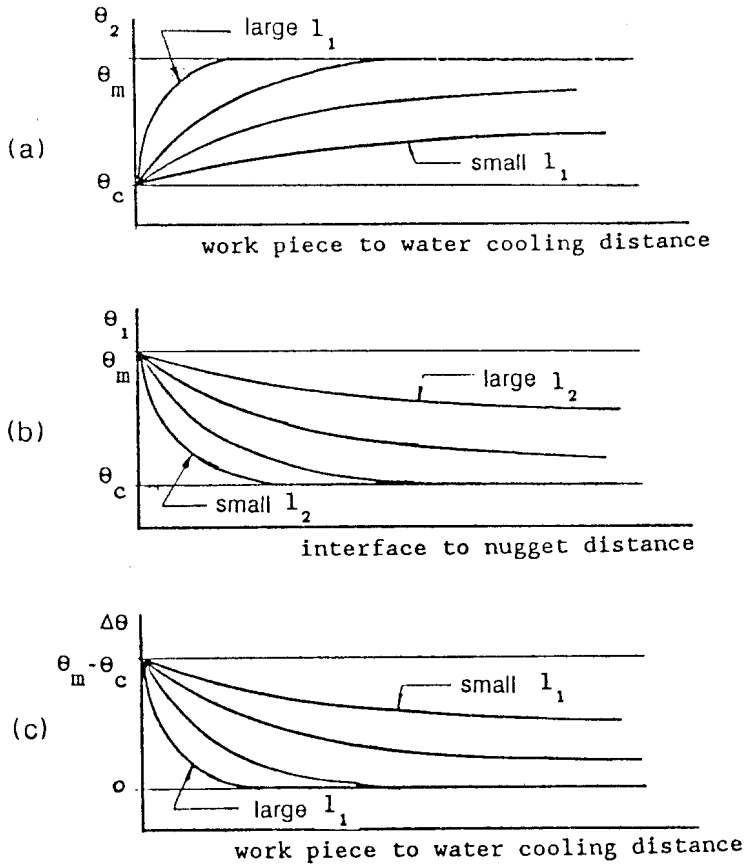

Figure 8: Change of Interface Temperature Due To a Geometrcal Change.

the same shape as given in reference 4. The position of the water jacket may also affect the interface temperature. The electrode-work piece interface exists all through the welding process and causes a temperature discontinuity at the interface with possibly a decreasing heat transfer resistance coefficient. This can be manifested by the easy separation of electrodes and work pieces at the end of the normal weld cycle. As the nugget develops, the distance l_1 decreases. For a given water jacket distance, l_2, the interface temperature at the work piece side, θ_1, approaches θ_m and increases the value of $\Delta\theta$ across the interface. However, as the temperature goes up, a softening of the material will occur and will reduce the interface thermal resistance. The water jacket distance, l_2, may also affect the temperature rise at the interface, and thus the heat loss across this interface varies in a very complex manner.

A rough comparison of heat loss in two directions can be made considering growth of the nugget. The ratio of axial heat loss, $\dot{Q}_a$, to the radial loss, $\dot{Q}_r$, is,

$$\frac{\dot{Q}_a}{\dot{Q}_r} = \frac{(\theta_m-\theta_1)al}{(\theta_m-\bar{\theta})2pl_1} \qquad (15)$$

Assuming nugget size growth is proportional to the geometry of the electrode and the thickness as explained in the model development section,

$$p = a\beta L/b \qquad (16)$$

where, p : penetration
β : final penetration to work piece thickness ratio (about 0.8)
b : electrode contact surface radius

Then the final ratio becomes,

$$\frac{\dot{Q}_a}{\dot{Q}_r} = \frac{(\theta_m-\theta_1)bl}{2(\theta_m-\bar{\theta})\beta Ll_1} \qquad (17)$$

Assuming the nugget front revises its position at every half cycle (1/120 sec) in AC welding,

$$\bar{\theta}/\theta_m = 0.9, \quad \text{when } 1-0.2\sqrt{\alpha t}-\sqrt{\alpha}\,/50,$$

α : thermal diffusivity of work pieces

$$\frac{\dot{Q}_a}{\dot{Q}_r} = \frac{(\theta_m-\theta_1)b\sqrt{\alpha}}{10\,\theta_m\beta Ll_1} \qquad (18)$$

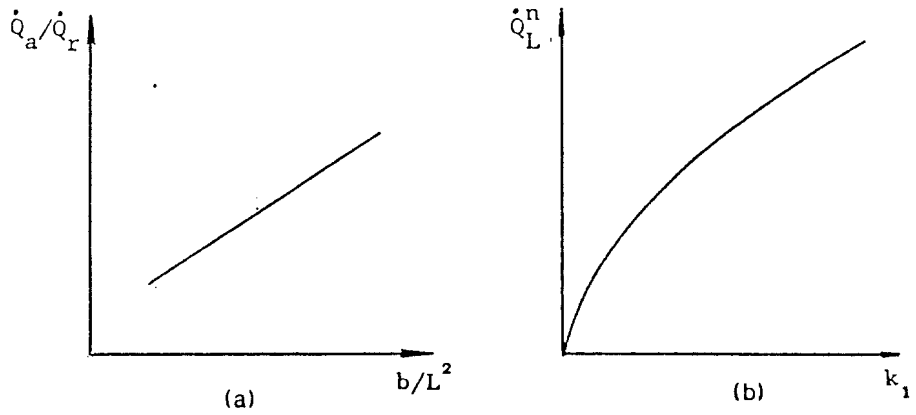

Figure 9: Characteristics of Heat Loss.

As l_1 reaches its final value abruptly, and if l_1 and θ_1 are assumed constant, the heat loss ratio in equation (18) is proportional to the parameter b/L^2. The effect of this parameter on the heat loss ratio is plotted in figure 9-a. The ratio is also a function of the thermal diffusivity, α.

The total heat loss can be described as follows using equations (9), (10) and (16).

$$\dot{Q}_L^n = \dot{Q}_a + \dot{Q}_r$$
$$= k_1\pi a^2[(\theta_m-\theta_1)/l_1+10(\theta_m\beta L)/(b\sqrt{\alpha})] \quad (19)$$

As the nugget diameter, a, increases with time, the rate of heat loss in the nugget, $\dot{Q}_L^n$, increases in a quadratic manner. But this should be compensated by changing the axial temperature gradient in the work piece, $(\theta_m-\theta_1)$, which seems to decrease with time. The thermal conductivity also affects the total heat loss as shown in figure 9-b.

It is almost certain from this analysis that the electrode geometry and the work piece thickness are very important factors not only in the distribution of the heat generation rate but also in determining heat dissipation characteristics of resistance spot welding. Generally, as one welds thinner sheet metal, the temperature gradients in the sheet become steeper and a greater portion of the total heat is lost to the electrodes.

MODEL CALCULATION

The lobe curve data used in this section is shown in figure 10 and are taken from reference 17. The material is G90 galvanized steel with a thickness of 1.5 mm. The electrode is a truncated cone type with 120 degrees included angle and 1/4 inch (6.4 mm) contact diameter with 15 mm face thickness and 16 mm outer diameter. The minimum accepable nugget size is 0.22 inches (2.8 mm) diameter. The experimentally determined lobe curve for this material is shown in figure 10-a; the dynamic current curve is in figure 10-b and the dynamic resistances are shown in figure 10-c and 10-d. Using this data, the calculation was performed for the case of no slope control in figure 10-a. The results are tabulated in table 1.

The total heat generated in the system was calculated assuming a linerized current value using the measured dynamic resistance. The heat required for phase changes were included in the calculation. The amount of heat required for nugget heating, Q_T^n, was calculated using heat capacity values, C_{pn}, from reference 18, which gives a value of 660J/kg •K. The heat used for the temperature rise in the electrodes was calculated using the simulated electrode surface temperature data from reference 4 and the measured surface temperature profile obtained by the authors [19]. The temperature profile on the electrode surface during welding is shown in figure 11. This was measured using an infrared emission monitoring system (Thermovision). This figure shows the transient temperature profile on both electrode surfaces which is approximately the maximum temperature experienced by the electrode face. The three profiles have about 10 millisecond time interval in the vertical direction. The horizontal direction is the axis of electrodes. The work pieces are in the center portion where the temperature valley lies. This is due to the low temperature of the outer edge of work piece. The highest electrode temperature used in the calculation is 400°C for a minimum nugget size and 450°C for a maximum size nugget.

In the calculation of heat loss, $\dot{Q}_L$, it was roughly assumed that no heat is lost through the model boundary till the nugget starts to form. It was also assumed that the temperature build up in the electrodes has already been reached when melting starts in the

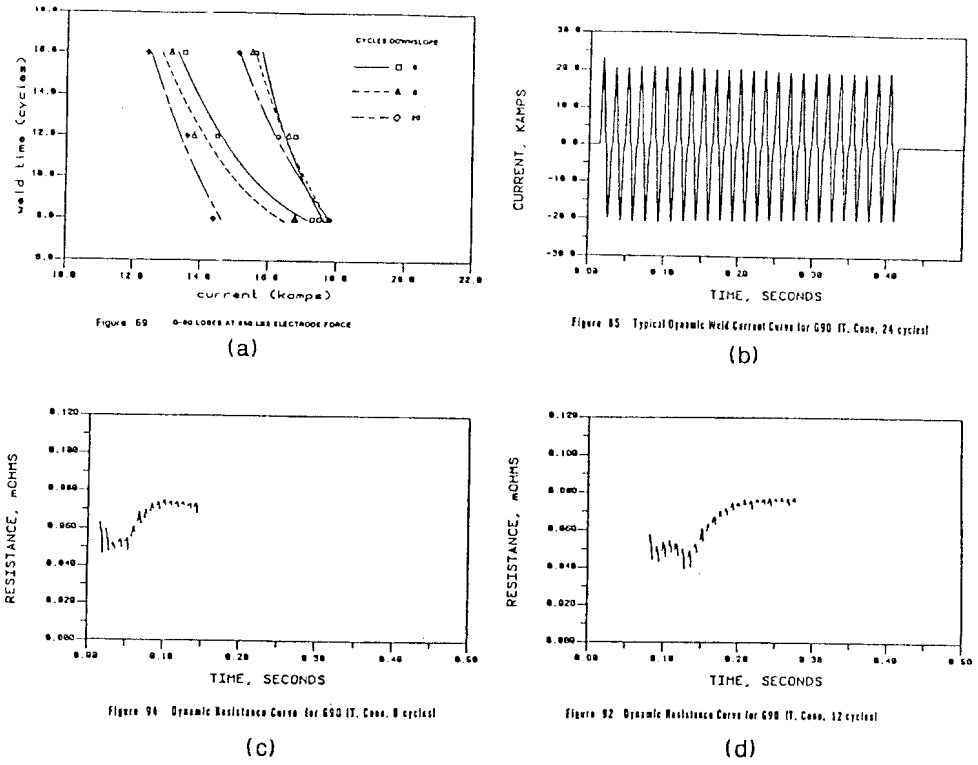

Figure 10: Welding Data for Calculation. (after ref. 17)

TABLE 1 : Proportion of Heat Consumption in RSW.

TERMS	5.6 mm nugget (MINIMUM)			6.4 mm nugget (EXPULSION)			SYMBOL, UNIT
weld time	8	12	16	8	12	16	Δt (cycle)
weld current	17.2	14.5	13.6	17.6	16.7	15.6	I (KAmp)
total resistance	0.07	0.07	0.07	0.07	0.07	0.07	R (mOhm)
total heat generation	2760 100%	2950 100%	3450 100%	2890 100%	3900 100%	4540 100%	Q_g (J)
nugget heating and melting	750 27%	750 25%	750 22%	1110 38%	1110 28%	1110 24%	$Q_T^n + H_f$ (J)
electrode heating	1520 55%	1520 52%	1520 44%	1610 56%	1610 41%	1610 35%	Q_T^e (J)
loss to cooling water	110 4%	120 4%	120 3%	170 6%	300 8%	410 10%	Q_L (J)
surrounding metal heating	380 14%	560 19%	1060 31%	0 0%	880 23%	1410 31%	Q_T^s (J)
t_1, t_3	3,5	6,9	9,13	3,5	4,6	6,8	(cycle)
interface temperature	500	500	500	700	700	700	θ_1 (°C)

nugget. After that time, the heat loss rate, $\dot{Q}_L$ is assumed to be equal to the axial heat loss rate, $\dot{Q}_a$, as discussed previously. This is due to the fact that the temperature gradient in the axial direction which developed before nugget melting occurs, is low compared to the gradient at later times. The heat loss into the work piece is included in the total amount of heat required for the temperature rise in the surrounding nugget material, Q_T^s.

The axial heat loss rate, $\dot{Q}_a$, derived in this paper is a function of the interface temperature, θ_1, and the nugget thickness or the nugget radius. The θ_1 value was estimated from reference 4 and was measured from the experimental data shown in figure 11. The relationship between time and nugget thickness (or nugget radius) can be found in references such as 4, 6 and 9. The nugget thickness change with time can be simplified as shown in figure 12. As the effect of an increase in current on the total amount of heat generated in the system is quadratic while the welding time is linear, welding with high current - short weld times will produce a steeper slope (see figure 12) as compared with welding with low current - long weld times. The shape of the curves is represented by three time values. The time t_1 is the melting start time, t_2 is the time at which 70% of the final nugget size is reached and t_3 is the time for the final nugget size. In some cases t_3 is equal to the weld time Δt. The values used are listed in table 1. The rate of axial heat loss, $\dot{Q}_a$, was then integrated over welding time.

The ratio of the axial and the radial heat loss rate from a nugget was calculated using equation 18. The result for the case of this calculation shows that the ratio is about 0.3 at the start of nugget formation and about 1.1 at the end of a full penetration nugget (defined as having a diameter equal to the electrode face diameter). The heat loss rate of a maximum size nugget is 2570 J/sec in the axial direction and 2250 J/sec in the radial direction.

DISCUSSION

According to the calculation done in the previous section, the net heat used for melting of the nugget is only 25% of the total heat generated in the process. Most of the heat is consumed in the electrodes and in heating up the surrounding sheet metal. The heat used for the temperature rise in electrodes, Q_T^e, is about 40 to 50 percent of the total heat. This comprises the heat from the work pieces and the heat generated in the electrode itself as assumed previously. The high portion of the heat lost to the electrodes is due to the large volume of electrodes. As the electrode face thickness in this calculation is 15 mm, most of the heat from the work piece goes into heating of the electrode. If the maximum temperature profile in the electrodes is assumed to be constant for each weld, the proportion of heat lost to the electrodes will decrease with

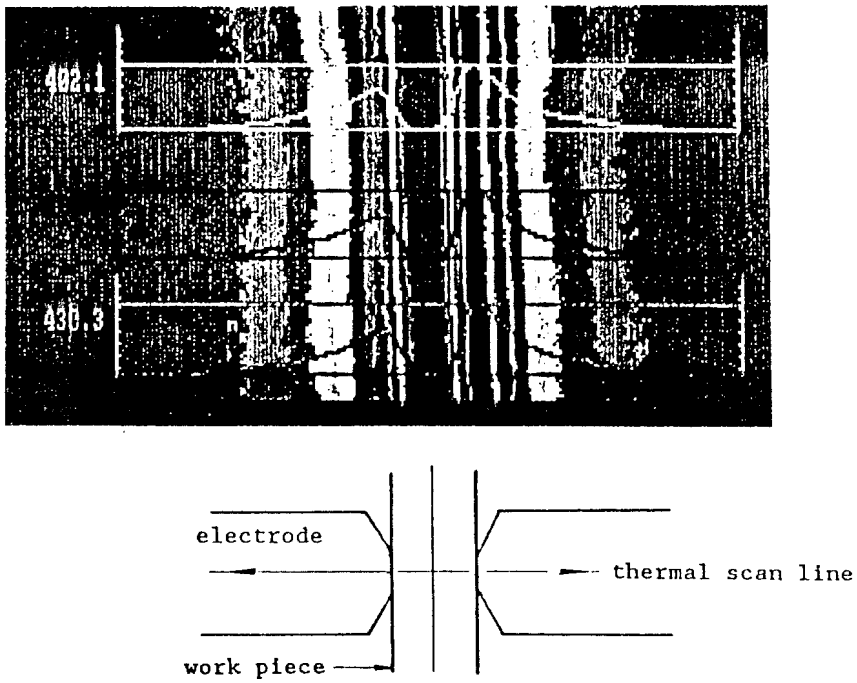

Figure 11: Temperature Profile on the Electrode Surface.

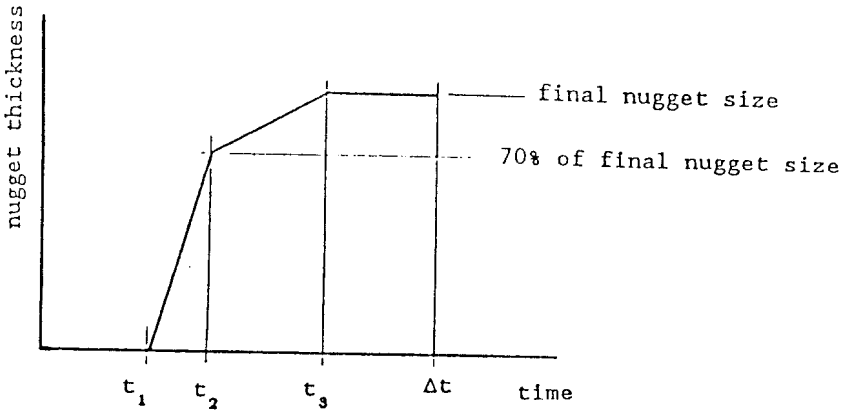

Figure 12: Characteristic Nugget Growth Curve

increasing weld time as shown in table 1. The proportion of heat lost to the surrounding nugget material and the cooling water will increase with increasing weld time. This is not a surprise because of the longer time for heat dissipation as the weld progresses.

The heat loss to the cooling water does not constitute a large proportion of the total heat in this calculation when compared to the radial loss in the sheet metal. This seems to be mainly due to the small aspect ratio of 1.1 of the electrode face diameter to the work piece thickness. In this case, the heat loss rate in both directions is almost the same at the end of the nugget development, while the heat loss rate in the radial direction is about four fold of the axial loss rate at the early stages of nugget growth.

If the heat loss rate is estimated for changes in geometrical factors, such as sheet thickness and electrode size, the ratio of the axial heat loss rate to the radial heat loss rate changes in proportion to the parameter b/L^2. By reducing the thickness by half, the ratio increases by a factor of four. For this case the radial heat loss rate alone decreases by a factor of two as indicated by equation (19). If the electrode diameter is doubled, the ratio increases by a factor of two while the axial heat loss rate increases by four fold. This means that a thinner work piece, e.g. 0.8 mm, will lose an even greater fraction of the heat by conduction into the electrode than has been estimated in Table 1 for a 1.5 mm thick sheet. Thus, heat transfer through the electrode-work piece interface will dominate the nugget growth mechanism in thin sheet welding. A very small variation in the contact characteristics may result in great inconsistancy in weldability. This will be more pronounced as the work piece thickness becomes less. This may also increase the maximum temperature which the electrode achieves or the length of time at this temperature. In addition, this may cause a large reduction in electrode life especially in galvanized steel welding.

If the thermal conductivity changes, the relevant terms such as heat loss rate through the model boundary, $\dot{Q}_L$, and the amount of heat required for temperature rise in the surrounding nugget material, Q_T^s, will be affected. The heat loss rate through the model boundary, $\dot{Q}_L$, is approximately equal to the axial heat loss rate, $\dot{Q}_a$, while Q_T^s is roughly the integral of the radial heat loss rate, $\dot{Q}_r$, over time. In equation (19), the axial heat loss rate, $\dot{Q}_L$, is proportional to $k_1 a^2/l_1$ and the radial heat loss rate, $\dot{Q}_r$, is proportional to $/k_1 a^2$. According to these relationships the shift of the expulsion lobe boundary will be larger than that of the minimum nugget boundary due to the difference in the nugget size, a. Therefore, if the thermal conductivity of the metal is increased, the lobe width will be increased along with a translation of the lobe in the direction of high energy input.

Material with high contact resistance, R_c, requires relatively less heat input. This may be due to the early temperature build up within the system before the start of nugget formation. This may also increase the lobe width, possibly due to an early start of nugget formation at low current levels. Specifically, the increase in the lobe width may be due to the larger increase in the total heat loss produced by larger size nuggets and the longer heat dissipation time.

The change of work piece bulk resistance, R_w, to a higher value will move the lobe position in the direction of lower energy input. From equation (6), it can be seen that this shift is greater when the nugget size is large. This will reduce the lobe width.

It is obvious that the lobe will shift in the direction of high energy input if the value of volumetric heat capacity, ρC_p, is increased. This can be easily seen from equation (5). If

nugget size is considered, the shift will be greater with a larger size nugget. Thus, a wider lobe width is possible if a material with a high volumetric heat capacity, ρC_p, is used.

It is seen that the ratio of material properties $\rho C_p/\sigma$ and k/σ could be important factors which affect the lobe shape. The increase in the volumetric heat capacity, ρC_p, and thermal conductivity of the work pieces, k, will increase the lobe width and will require a larger total heat input. On the contrary, an increase in electrical resistivity will decrease the lobe width and the total amount of heat necessary to form a nugget. Therefore, these two ratios can be used as parameters to describe the weldability of a specific material. In general, it can be said that a material with large values of these ratios will have a wider lobe width and will require a higher energy input.

Different combinations of weld time, Δt, and weld current, I, will have different effects on the lobe shape. Welding with high current at short nugget growth times, $(\Delta t - t_1)$, will result in a smaller heat loss to the surroundings as discussed in the model calculation section. On the contrary, long weld times with lower currents will produce greater heat loss. As this will demand a higher heat input for the same sized nugget, the slope of the lobe curve in this region will become steeper. This can also explain the reason why the lobe is wider in the long weld time region.

Thus far it was assumed that heat transfer through the electrode-work piece interface is not a rate controlling step. If the interface has very high thermal resistance, the heat loss to the electrode will be reduced and the lobe width will decrease. This may be the case with hard materials such as high strength low alloy steel compared to a low carbon steel. The experimental data in reference 20 support this argument.

CONCLUSION

A parametric heat flow analysis of the resistance spot welding process shows that:

1. The ratio of the heat loss rate in the electrode compared to the heat loss rate in the work piece is a function of the electrode diameter divided by the square of the work piece thickness.

2. Small variations in the electrode-work piece thermal contact characteristics can result in a great inconsistancies in the weldability of thin sheets.

3. The ratio of thermal conductivity and heat capacity to electrical resistivity is a characteristic number which is representative of the ease of spot weldability of a given material. The increases in thermal conductivity and heat capacity of the sheet metal increase the lobe width while increases in electrical resistivity decrease the lobe width.

4. Welding with a high electrical contact resistance will increase the lobe width provided that increasing this resistance does not produce expulsion at the electrode-sheet interface.

5. The wider lobe width of long time - low current welds can be explained by the larger amount of total heat dispission due to the longer weld time and the larger heat loss area of larger nuggets.

REFERENCES

1. D. W. Dickinson, 'Welding in the automotive industry', Report SG 81-5, Committee of Sheet Steel Industries, AISI, Aug., 1981.
2. H. A. Nied, 'The finite element modeling of the resistance spot welding process', Welding Journal, pp.123s-132s, April, 1984.
3. J. A. Greenwood, 'Temperatures in spot welding', British Welding Journal, pp.316-322, June, 1961.
4. A. F. Houchens, R. E. Page, W. H. Yang, 'Numerical modeling of resistance spot welding', Numerical modeling of manufacturing process, edited by R. F. Jones Jr., D. W. Taylor, H. Armen, J. T. Hong, ASME, pp.117-129, 1977.
5. W. Rice, E. J. Funk, 'An analytical investigation of the temperature distribution during resistance welding', Welding Journal, pp.175s-186s, April, 1967.
6. J. E. Gould, 'An experimentation of nugget development during spot welding, using both experimental and analytical technique', Welding Journal, pp.1s-10s, Jan., 1987.
7. G. R. Archer, 'Calculation for temperature response in spot welds', Welding Journal, pp.327s-330s, Aug., 1960.
8. K. P. Bentry, J. A. Greenwood, P. McK Knowlson, R. G. Baker', Temperature distribution in spot welds', British Welding Journal, pp.613-619, Dec., 1963.
9. K. Nishiguchi, K. Matsuyama, 'Influence of current wave form on nugget formation phenomena in spot welding of thin sheet', IIW doc. No. III-805-85, IIW, 1985
10. S. P. Owusu-Ofori, S. M. Wu, 'Signiture analysis of contact voltage of resistance welds', Welding Journal, pp.185s-189s, July, 1983.

11. S. Nakada, M. Nishikawa, M. Kawasaki, J. Horie, M. Juri, 'In-process quality control of spot weld by detecting voltage between electrode tips', Proceedings of International Conference on Welding Research in the 1980's, Section B, pp.251-256, International Conference Commettee, Osaka, Japan, Sep., 1980,
12. J. Kelly, P. M. Knowlson, 'The BWRL quality monitor and spot-welding galvanized steel sheet - an evaluation', Welding Journal, pp.114s-120s, March 1967.
13. D. G. Waters, K. -C. Lee, R. J. Mayhan, D. W. Dickinson, 'A microcomputer based sensor system for resistance welding studies', Conference Proceedings, Sheet Metal Welding Conference, Paper No.13, AWS, 1984.
14. J. M. O'Brien, 'Adaptive feedback control for galvanized welding', Conference Proceedings, Sheet Metal Welding Conference, Paper No.26, AWS, 1984.
15. I. L. Hawkins, Superior quality production spot welding using adaptive control', Conference Proceedings, Sheet Metal Welding Conference, Paper No. 22, AWS, 1984.
16. D. W. Dickinson, J. E. Franklin, A Stanya, 'Characterization of spot welding behavior by dynamic electrical parameter monitoring', Welding Journal, pp.170s-176s, June, 1980.
17. S. A. Gedeon, 'Resistance spot welding of galvanized steel sheet', M.S. Thesis, Massachusetts Institute of Technology, 1984.
18. Y. S. Touloukian et al, Thermophysical properties of matter, metallic elements and alloys, Plenum, 1973.
19. E. W. Kim, T. W. Eagar, unpublished work at MIT.
20. J. G. Kaiser, G. J. Dunn, T. W. Eagar, 'The effect of electrical resistance on nugget formation during spot welding', Welding Journal, pp.167s-174s, June, 1982.

ACKNOWLEDGEMENT

We wish to acknolwedge the financial support of General Motors, Ford Motor Co., and the Internal Lead Zinc Research Organization for this work.